Journal of Catalysis 260 (2008) 65–74

Contents lists available at ScienceDirect

Journal of Catalysis

www.elsevier.com/locate/jcat

Structure, stability and activity of RuS_2 supported on alumina

Perla Castillo-Villalón [a], Jorge Ramírez [a,*], Françoise Maugé [b]

[a] UNICAT, Departamento de Ingeniería Química, Facultad de Química, Universidad Nacional Autónoma de México, Cd. Universitaria, México, D.F., 04510, Mexico
[b] Laboratoire Catalyse et Spectrochimie, ENSICAEN, Université de Caen, CNRS, 6 Bd Maréchal Juin, 14050, Caen, France

ARTICLE INFO

Article history:
Received 25 June 2008
Revised 28 August 2008
Accepted 28 August 2008
Available online 1 October 2008

Keywords:
Ru/Al_2O_3 catalysts
TPR-S
Thiophene hydrodesulfurization
Ruthenium sulfide

ABSTRACT

The relationships between the structure attained by alumina-supported RuS_2 during sulfidation, the extent of desulfurization of the sulfided phase during HDS, and the hydrodesulfurization activity of the catalyst were studied by TPS, TPR-S, XRD, FT-IR of CO, and DRS–UV–Vis–NIR. Sulfidation in H_2S/N_2 generates a mixture of RuS_2-pyrite and RuS_2-amorphous. As the sulfidation temperature increases, more RuS_2-pyrite is produced at the expense of RuS_2-amorphous. The later is not stable and undergoes reduction in reaction conditions, producing a sulfur-depleted catalyst ($S/Ru < 2$) with low HDS activity. In contrast, RuS_2-pyrite resists the drastic reducing conditions prevailing during HDS and is responsible for the high HDS activity. The changes in the catalyst properties with sulfidation temperature produce an opposite trend in the hydrogenation activity of naphthalene. The structure of the ruthenium sulfide catalyst can be tuned during sulfidation to achieve optimum performance according to the hydrodesulfurization or hydrogenation requirements of the reaction system.

1. Introduction

Bulk ruthenium sulfide is the most active catalyst in the hydrodesulfurization of such molecules as thiophene, dibenzothiophene (DBT), and 4,6-dimethyldibenzothiophene (4,6-DMDBT) compared with other transition metal sulfides [1–4]. The difference in catalytic activity between RuS_2 and MoS_2 or WS_2 (used in conventional HDS catalysts) is at least of one order or magnitude. In addition, RuS_2 is the only sulfide that produces cyclohexylbenzene in the HDS of DBT, demonstrating its hydrogenating capability. The study of this feature with the biphenyl hydrogenation reaction showed that bulk RuS_2 is five times more active than bulk MoS_2 or WS_2 [5]. Clearly, RuS_2 has characteristics of interest to the elimination of the most refractory sulfur compounds present in transport fuels, because the transformation of these compounds occurs mainly through a hydrogenation–hydrodesulfurization reaction route. The behavior of supported ruthenium sulfide catalysts is not yet completely understood, however.

The sulfidation behavior of ruthenium in supported catalysts has some interesting features. Previous studies on the sulfidation of alumina-supported Ru metallic particles showed that obtaining RuS_2 with pyrite structure both in surface and bulk requires drastic sulfidation treatment (i.e., high temperature [$T > 700$ K] and high H_2S concentrations [>80%]) when the sulfidation is performed in a H_2S/H_2 stream [6–10]. The results also showed that it is more difficult to obtain pyrite structure on the surface of the supported RuS_2 particles than in the bulk. Thus, it is not uncommon to produce RuS_2 particles with pyrite structure in the bulk but not on the surface [6–10]. It is interesting that once the RuS_2 particle has achieved the pyrite structure both on the surface and in bulk, it is stable and remains unaltered when placed in a stream with lower H_2S/H_2 ratios at high temperatures, in agreement with thermodynamic calculations that established that few ppm of H_2S in a H_2 stream are sufficient to maintain RuS_2 sulfided [11].

The sulfidation procedure has a significant influence on the HDS activity of ruthenium-supported catalysts [12]. For example, if alumina-supported $RuCl_3 \cdot xH_2O$ is first reduced and then sulfided with $H_2S(15\%)/N_2$, then the catalyst displays half the activity of the catalyst prepared by avoiding the reduction step. Furthermore, the sulfidation of alumina-supported $RuCl_3 \cdot xH_2O$ with $H_2S(15\%)/N_2$ at 673 K gives rise to a catalyst that is much more active in the HDS of thiophene than that obtained by the typical sulfidation procedure using $H_2S(15\%)/H_2$ at 673 K. These results clearly show the negative effect of hydrogen during the sulfidation of a ruthenium-based HDS catalyst [13,14].

The sulfidation of alumina-supported $RuCl_3 \cdot xH_2O$ at 673 K with $H_2S(15\%)/H_2$ gives rise to an active phase with a S/Ru ratio < 2, RuS_{2-x}, conformed by RuS_2 and small domains of metallic ruthenium [15]. In contrast, sulfiding with $H_2S(15\%)/N_2$ or pure H_2S leads to better sulfidation, generating an active phase with S/Ru ratio > 2, RuS_{2+x} [16–18]. Because the only stable sulfide of ruthenium is RuS_2 [19–21], the observed excess of sulfur was assigned to overstoichiometric sulfur retained on the catalyst during the sulfidation process as S^0 and/or S_x, with sulfur completing the coordination sphere of superficial Ru in RuS_2 [22,23].

* Corresponding author. Fax: +52 55 56 22 53 66.
E-mail address: jrs@servidor.unam.mx (J. Ramírez).

0021-9517/$ – see front matter
doi:10.1016/j.jcat.2008.08.015

The composition of the sulfidation stream is not the only factor influencing the HDS activity. When alumina-supported $RuCl_3 \cdot xH_2O$ is sulfided with $H_2S(15\%)/N_2$, the catalytic activity in the HDS of thiophene shows a strong dependence on the sulfidation temperature; increasing the sulfidation temperature from 573 to 873 K leads to better HDS catalytic performance [16]. Because the increase in sulfidation temperature can lead to larger sulfided particles (poorer dispersion of the active phase), it has been proposed that the observed increase in HDS activity resulted from large RuS_2 particles preferentially exhibiting (210) planes, which are more active in HDS, whereas small particles exhibit mostly (111) faces, more active in hydrogenation reactions.

A relevant characteristic of ruthenium sulfide produced at 673–773 K in $H_2S(15\%)/N_2$ is its significant reduction in hydrogen atmospheres at temperatures close to those used in HDS reaction (493–593 K). The extent of reduction of silica-supported ruthenium sulfide in hydrogen atmosphere goes from 13 to 100% at temperatures from 423 to 673 K [22]. Moreover, temperature-programmed reduction (TPR) experiments have shown that at 493–593 K, the reduction of alumina- and silica-supported RuS_2 goes from 1/3 to 2/3 of the entire RuS_2 reduction. When RuS_2 is dispersed inside a zeolite (KY, HY) the reduction at 493–593 K involves almost all of the RuS_2 present in the catalyst [17,23–25]. Comparison of bulk MoS_2 and RuS_2 in TPR experiments revealed that at 1000 K, only 10% of MoS_2 is reduced, whereas at 830 K, RuS_2 is completely reduced [26].

Although the aforementioned reduction and TPR experiments were performed in pure or diluted hydrogen, it is worth investigating whether RuS_2 suffers a similar reduction when placed in the reductive reaction stream prevailing during HDS. Some reports have indicated a strong desulfurization of RuS_2 supported in MgF_2 prepared at 673 K in $H_2S(50\%)/N_2$ during the HDS of thiophene [27]. The same effect was observed in KY zeolite supported RuS_2 sulfided with $H_2S(15\%)/N_2$ at 673 K during the hydrodenitrogenation of pyridine [28]. An EXAFS study revealed that in the case of RuS_2/KY sulfided under the same conditions, small domains of metallic ruthenium are present on the catalysts after tetraline hydrogenation, despite the ∼2% H_2S added to the reaction stream [15]. It appears then that to gain insight into the behavior of alumina-supported RuS_2 catalysts, a systematic study of the reduction of RuS_2 during the HDS reaction is needed.

The results from the literature show that ruthenium sulfide catalysts supported on alumina display different hydrodesulfurization activities depending on the sulfidation procedure, composition of the sulfiding stream, and sulfidation temperature. But whether this behavior is related to changes in the structure of the Ru sulfide phase is not clear, because only changes in the catalyst composition were reported. In particular, it has not been clearly established whether the desulfurization of the sulfided phase and the appearance of metallic ruthenium domains reported after reaction positively or negatively affect the catalytic performance in HDS. It also remains unclear whether the extent of desulfurization is a consequence of the structure attained by the ruthenium sulfide during sulfidation, or whether the same degree of desulfurization is associated with high activity in hydrodesulfurization and hydrogenation reactions.

The object of the present work was then to determine the relationships between the structure attained by the alumina-supported Ru sulfide phase during sulfidation, the extent of desulfurization of the ruthenium sulfide phase during the HDS reaction, and the hydrodesulfurization activity displayed by the catalyst. Toward this end, a detailed TPS and TPR-S study of a Ru/Al_2O_3 catalyst sulfided at different temperatures was carried out. A thorough characterization of the nature of the Ru sulfided phases obtained at different sulfidation temperatures was performed by XRD, FT-IR of CO adsorbed at low temperature, SEM-EDS, TEM, and DRS–UV–Vis–NIR. The findings of this study were related to the catalyst activity and selectivity in hydrodesulfurization and aromatic (naphthalene) hydrogenation reactions. Thiophene was chosen as model molecule for the HDS tests because, being small, it can easily reach the active sites and do not present impediment for adsorption; therefore, all changes in the active phase can manifest as changes in activity.

2. Experimental

2.1. Catalyst preparation

Ru/Al_2O_3 with nominal content of 2.1 ruthenium atoms per square nanometer of Al_2O_3, equivalent to 7 wt% Ru, was prepared using $RuCl_3 \cdot 3H_2O$ (Aldrich) as precursor. γ-Al_2O_3 support with surface area 238 m^2/g, pore volume 0.52 cm^3/g and average pore size 87 Å was obtained by calcination of boehmite Catapal-B at 823 K for 4 h (heating rate, 3 K/min).

To prepare the catalyst, $RuCl_3 \cdot 3H_2O$ was dissolved in 2.5 times the volume of water required to obtain incipient wetness (2.5 × 1 ml/g Al_2O_3). The solution was maintained under stirring for 12 h in N_2, after which the alumina was added and the suspension stirred for another 12 h. The catalyst was dried first in air flow at room temperature to eliminate the excess liquid and then in an oven at 383 K for 24 h. The solid was stored in a vacuum desiccator and used without further drying for the experiments.

For thiophene HDS, naphthalene hydrogenation, and characterization, the catalyst was sulfided for 2 h at different sulfidation temperatures (573, 673, 773 or 973 K) in a 15 ml/min $H_2S(15\%)/N_2$ stream.

2.2. Catalytic tests

2.2.1. Thiophene hydrodesulfurization (HDS)

The catalytic tests were performed at atmospheric pressure in a continuous-flow microreactor. The reaction products were analyzed by online gas chromatography using an HP 5890 Series II gas chromatograph. Before the catalytic tests, the catalyst (100 mg) was sulfided *in situ* for 2 h. After the 2-h sulfidation, the catalysts were cooled to a reaction temperature of 633 K in $H_2S(15\%)/N_2$ and then contacted with a 20 ml/min stream of hydrogen saturated with thiophene at 275 K. In the case of sulfidation at 573 K, the catalyst was contacted with the reaction stream at the sulfidation temperature and then heated to 633 K. Initially, the catalyst was maintained at the reaction temperature of 633 K until no conversion change was observed (∼15 h), followed by measurements of thiophene conversion at different temperatures (from 493 to 593 K).

2.2.2. Naphthalene hydrogenation (HYD)

The reaction was carried out in a 300-ml Parr batch reactor operating at 950 psig of H_2, 593 K, and 700 rpm with 10% naphthalene, 85.8% *n*-decane, and 4.2% CS_2 (3.5% S). Catalyst sulfidation (150 mg) was performed in a flow microreactor as described in Section 2.1. The sulfided catalyst was transferred to the batch reactor in Ar atmosphere. The products after 24 h of reaction were analyzed by gas chromatography (HP 5890 Series II).

2.3. Characterizations

2.3.1. Temperature-programmed sulfidation (TPS) and reduction (TPR-S)

The experiments were carried out in a flow system equipped with a microreactor online with a Varian Cary 50 UV–Vis spectrometer to measure the evolution of H_2S at a fixed wavelength of 200 nm, and with a Gow-Mac thermal conductivity detector (TCD)

to evaluate the amount of H_2 consumed during the sulfide reduction. TPS patterns were registered during the sulfidation of the catalyst by monitoring the H_2S evolution versus temperature with UV–Vis. The TPR-S experiments were carried out with 150 mg of catalyst freshly sulfided and with samples tested in thiophene HDS. The catalyst was heated in a 25-ml/min stream of H_2 (70 vol%)/Ar at a constant rate of 10 K/min from room temperature to 1273 K. The reactor outlet stream was monitored by UV–Vis and, after removal of H_2S in a trap, by TCD.

2.3.2. X-ray diffraction

X-ray diffractograms of sulfided catalysts were registered with a Phillips 1050/25 diffractometer using Cu$K\alpha$ radiation ($\lambda = 1.5418$ Å) and a goniometer speed of $1^\circ\,(2\theta)\,\mathrm{min}^{-1}$.

2.3.3. Scanning electron microscopy (SEM)

After 15 h under HDS reaction at 633 K, the sulfided catalysts were analyzed by SEM in a JEOL 5900-LV equipped with an Oxford EDS system.

2.3.4. Transmission electron microscopy (TEM)

The sulfided samples after 15 h under thiophene reaction at 633 K were observed in a JEOL 2010 microscope. To avoid contact with air, the catalyst powder was transferred directly from the reactor filled with N_2 to a vial filled with *n*-heptane. One drop of the suspension catalyst–*n*-heptane was placed in a copper grid with carbon lacey, and, after evaporation in air, the sample was introduced in the microscope.

2.3.5. FT-IR spectroscopy of CO adsorbed at ∼100 K

For infrared spectroscopy, the catalyst was pressed into self-supported discs (8.5 mg/cm^2). The analysis was conducted using a Nicolet Magna 760 spectrometer with 2 cm^{-1} resolution. The experiment involved two successive steps: (a) characterization of the freshly sulfided sample and (b) characterization after the catalyst was maintained for 10 h in an environment close to that encountered under HDS, that is, 633 K in a continuous flow (20 ml/min) of $H_2S(15\%)/H_2$. The conditions used to simulate the HDS reaction in the CO adsorption experiments are similar to the real conditions in terms of the treatment temperature, the reductive environment, and the presence of H_2S in the gas stream.

The self-supported wafer was placed in a low-temperature infrared transmission cell equipped with CsF_2 windows and double walls for liquid nitrogen. Sulfidation of the sample was done *in situ* under $H_2S(15\%)/N_2$ as described in Section 2.1, cooled to room temperature, and flushed with nitrogen. The sulfided catalyst was then outgassed under vacuum at 673 K for 4 h. Calibrated doses of CO (0.03, 0.08, 0.16, 0.31, 0.31, 0.78, 1.56, 3.12 µmol) were successively contacted with the catalyst at ∼100 K. A spectrum was obtained after each addition. Finally, one spectrum was obtained at 1 Torr of CO in equilibrium with the sample, and another was obtained after several minutes of evacuation at ∼100 K. To prepare the sample for the next part of the experiment, CO was desorbed from the catalyst with vacuum at room temperature.

For characterization of the catalyst wafer treated at conditions similar to HDS (20 ml/min of $H_2S(15\%)/H_2$ at 633 K for 10 h), the sample was resulfided for 1 h as described in Section 2.1. Then the same characterization procedure described in the previous paragraph was followed.

2.3.6. DRS–UV–Visible–NIR spectroscopy

The spectra of freshly sulfided catalysts were obtained with a Cary 500 Varian spectrometer equipped with a diffuse reflectance sphere.

Table 1
Thiophene HDS activity of sulfided Ru/Al_2O_3.

Sulfidation temperature (K)	$r \times 10^3$ (molecule of thiophene s^{-1} (Ru atom)$^{-1}$)	$r \times 10^{10}$ (molecule of thiophene s^{-1} m^{-2})
	Sulfided in $H_2S(15\%)/N_2$	
573	0.17	0.85
673	0.94	4.72
773	1.28	6.43
973	1.73	8.69
	Sulfided in $H_2S(15\%)/H_2$	
673	0.13	0.65

Note. Reaction rate at 553 K.

Table 2
Kinetic coefficient in naphthalene hydrogenation with Ru/Al_2O_3 sulfided in $H_2S(15\%)/N_2$.

Sulfidation temperature (K)	k[a] ($L\,g_{Ru}^{-1}\,h^{-1}$)
673	2
773	0.5
973	0.3

[a] Reaction conditions: 593 K, 950 psig H_2.

3. Results and discussion

3.1. Catalytic activity

Ru/Al_2O_3 catalysts sulfided at 573, 673, 773, and 973 K in $H_2S(15\%)/N_2$ were tested in the HDS of thiophene. From the activity results at 493–593 K, an activation energy of about 64.7 kJ mol^{-1} was obtained for all catalysts. Hereinafter, only the activity at 553 K is reported.

The thiophene HDS activity increased with increasing sulfidation temperature from 573 to 973 K (Table 1). In contrast, the hydrogenation of naphthalene (represented by the kinetic coefficient) decreased with the sulfidation temperature (Table 2), demonstrating an opposite trend to thiophene HDS. These activity trends are in agreement with previous findings [16].

During thiophene HDS, a RuS_2 surface with pyrite structure has high selectivity toward tetrahydrothiophene [8,9]. In our experiments, the selectivity to tetrahydrothiophene (k_{HYD}/k_{HDS}) increased from 1.7 to 7.4 when the sulfidation temperature changed from 573 to 973 K, suggesting the progressive formation of pyrite structure on the surface of the RuS_2 particles with increasing sulfidation temperature. The increase in HDS activity with the sulfidation temperature also could be related to the structural changes induced by the sulfidation temperature in the RuS_2-supported particles. To explore this possibility, we analyzed the sulfidation and reduction behavior of the catalysts and performed a detailed characterization of the sulfided Ru/Al_2O_3 catalysts.

3.2. Sulfidation of Ru/Al_2O_3

TPS experiments were conducted to detect the existence of changes in the catalyst sulfiding pattern in the high temperature region. However, the TPS pattern displayed in Fig. 1 shows only one main H_2S consumption peak with a minimum at about 365 K, which corresponds to the formation of the sulfided Ru species. In fact, the trace reaches the baseline at about 600 K and remains stable during the rest of the experiment (heating up to 973 K followed by 2 h at 973 K, not shown) with no significant H_2S consumption at temperatures above 600 K. This indicates that the sulfidation of ruthenium takes place at temperatures below 600 K (peak at 365 K), and also shows the absence of significant amounts of other Ru species more difficult to sulfide. This result is in agreement with the in situ XAS characterization of the reductive sulfida-

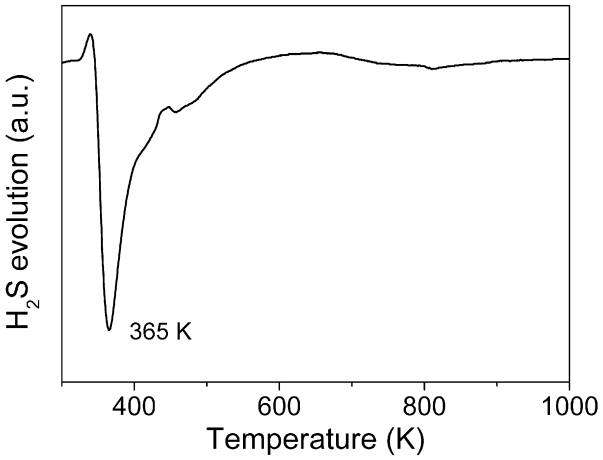

Fig. 1. TPS pattern of Ru/Al_2O_3 sulfided up to 973 K in $H_2S(15\%)/N_2$.

tion of a Ru/zeolite catalyst using $H_2S(15\%)/H_2$ as sulfiding stream, where the sulfidation of ruthenium was complete at 373 K [29].

According to these experiments, significant differences in the activity of Ru/Al_2O_3 catalysts sulfided at temperatures above 600 K should not be expected; however, as mentioned above, this was not the case. In fact, thiophene HDS activity increased 10-fold with increasing sulfidation temperature from 573 to 973 K (Table 1). In contrast, for naphthalene hydrogenation, the kinetic coefficient decreased by more than sixfold with increasing sulfidation temperature from 673 to 973 K (Table 2). Thus, the observed differences in catalytic activity should be related to structural changes in the Ru sulfided phase induced by the sulfidation temperature rather than to differences in the degree of Ru sulfidation.

3.3. X-ray diffraction of the sulfided catalysts

To analyze the possible changes in crystallinity induced by the sulfidation temperature, we conducted an XRD study. The XRD patterns of alumina and Ru/Al_2O_3 catalysts sulfided at the different temperatures are displayed in Fig. 2. An asterisk (∗) indicates the positions at which the diffraction peaks for RuS_2-pyrite are located. A vertical dashed line indicates the position of the main RuS_2-pyrite peak at $2\theta = 32°$.

The diffraction pattern of alumina shows two broad diffraction peaks at $2\theta = 45.7°$ and $2\theta = 66.8°$. Between $2\theta = 25°$ and 42.5°, a diffraction envelope, characteristic of an amorphous material, is found. Both features in the diffraction pattern indicate that alumina is partially amorphous.

The diffraction pattern of the catalyst sulfided at 573 K does not present any well-defined peak that could be related to RuS_2. However, a detailed analysis of the diffractogram shows that the ratio between the intensity of the alumina peak at $2\theta = 66.8°$ and the intensity of the diffraction envelope at the position of the main RuS_2 peak ($2\theta = 32°$) diminishes from 3.8 in the alumina support to 2.5 in the catalyst sulfided at 573 K, indicating some contribution to the amorphous diffraction envelope coming from RuS_2. Moreover, as the sulfidation temperature is increased, well-defined peaks of RuS_2-pyrite evolve from the diffraction envelope (see Fig. 2), and the intensity ratio $I_{2\theta=66.8}/I_{2\theta=32}$ diminishes even more (Table 3), indicating an increase in the quantity of RuS_2-pyrite diffraction centers. Thus, increasing the sulfidation temperature improves the crystallization degree of the ruthenium sulfide phase; however, it is not possible to establish from our XRD experiments whether RuS_2-pyrite is being formed on the surface of the ruthenium sulfide particles.

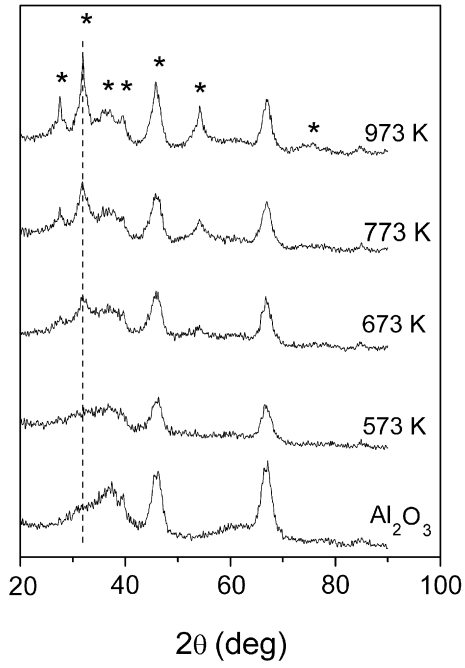

Fig. 2. XRD patterns of Al_2O_3 and Ru/Al_2O_3 sulfided at 573, 673, 773 and 973 K.

Table 3
Intensity ratio of the XRD peak of alumina at $2\theta = 66.8°$ and the diffraction envelope at $2\theta = 32°$ (main RuS_2-pyrite peak).

	$I_{2\theta=66.8°}/I_{2\theta=32°}$ ($I_{\text{peak } Al_2O_3}/I_{\text{peak } RuS_2}$)
Al_2O_3	3.8
RuS_2/Al_2O_3 ($T_{SULF} = 573$ K)	2.5
RuS_2/Al_2O_3 ($T_{SULF} = 673$ K)	1.3
RuS_2/Al_2O_3 ($T_{SULF} = 773$ K)	0.8
RuS_2/Al_2O_3 ($T_{SULF} = 973$ K)	0.6

3.4. Reducibility of RuS_2/Al_2O_3

TPR-S experiments were performed with Ru/Al_2O_3 sulfided at 573, 673, 773, and 973 K. In the TPR-S experiments the TCD (hydrogen consumption) and UV (H_2S production) traces followed the same trend, indicating the absence of significant contributions to the TPR-S patterns from processes like H_2S desorption, recombination of surface SH groups, or the presence of oxide Ru species. Therefore, only the UV trace is presented in this work.

Fig. 3 shows the TPR-S patterns obtained with the freshly sulfided catalyst. To facilitate the description and analysis, the TPR-S patterns were divided in two temperature zones, a low-temperature zone (Fig. 3A) from ambient temperature to 633 K, and a high-temperature zone (Fig. 3B) from 633 to 1273 K. The temperature chosen to divide both zones (633 K) was that used during the thiophene HDS experiments to reach the steady-state operation of the catalysts during the reaction (see Section 2).

The TPR-S patterns of catalysts sulfided at 573, 673, 773, and 973 K differed greatly from one another (Fig. 3). The amount of H_2S evolving from species that reduce at high temperature changes from 0.11 to 0.23 mmol, in detriment to some of the species that reduce at low temperature, where the amount of H_2S evolved decreases from 0.15 to 0.05 mmol (Table 4). Because the total amount of evolved H_2S remains almost constant (∼0.26 mmol), it seems that because of the increase in sulfidation temperature, some of the Ru sulfided species originally observed in the low-temperature zone of the TPR-S pattern are transformed into more stable RuS_2 species, which reduce at higher temperatures, and thus appear in the high-temperature region of the TPR-S patterns.

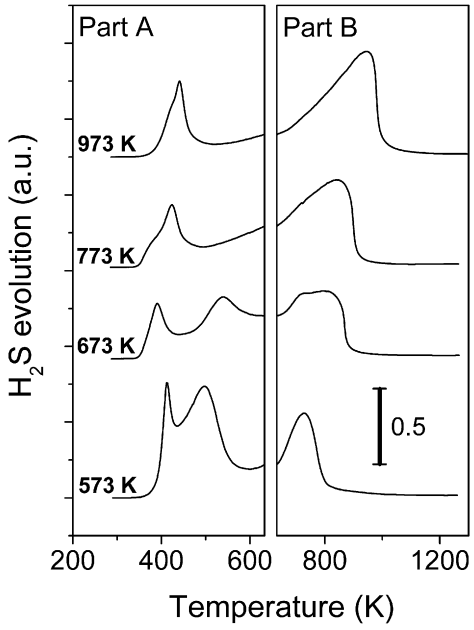

Fig. 3. TPR-S of Ru/Al_2O_3 freshly sulfided at 573, 673, 773 and 973 K. (A) Low temperature reduction and (B) high temperature reduction.

Table 4
H_2S evolution in the two reduction zones in TPR-S of freshly sulfided catalysts.

Sulfidation temperature (K)	H_2S evolved at $T < 633$ K (mmol)	H_2S evolved at $T > 633$ K (mmol)	Total H_2S (mmol)
573	0.15	0.11	0.26
673	0.10	0.15	0.25
773	0.08	0.19	0.27
973	0.05	0.23	0.28

In the low-temperature zone (298–633 K), Fig. 3A, the first peak with a maximum at ~415 K is assigned to the reduction of overstoichiometric sulfur, that is, elemental sulfur deposited on the catalytic surface due to the lack of hydrogen during sulfidation [16–18] and/or to sulfur coordinated to surface Ru [22,23]. The reduction of stoichiometric ruthenium sulfide then begins at 430–490 K. Fig. 3 shows that the reduction of stoichiometric RuS_2 is conformed by peaks whose intensity and position depends on the sulfidation temperature of the catalyst. In the pattern of the catalyst sulfided at 573 K, two main peaks are present at ~513 and 728 K. The first peak tends to disappear with the increment in sulfidation temperature, and thus the species responsible of this peak are not longer present in the catalyst after sulfidation at the higher temperature (973 K). This behavior strongly suggests that this peak arises from reduction of an amorphous or poorly crystallized Ru sulfide phase. The existence of amorphous RuS_2 has been clearly established in the literature, and some of its catalytic properties have been described earlier [30,31]. It appears that the poorly crystallized phase is formed at low temperature in the Ru/Al_2O_3 catalyst, as evidenced in our TPS experiments, and that higher temperatures are needed to induce crystallization into RuS_2-pyrite. Then, the peak with maximum around 513 K in Fig. 3A would correspond to the reduction of RuS_2-amorphous, which will transform into the more stable RuS_2-pyrite as the sulfidation temperature is increased. Therefore, the growing asymmetric peak in the high-temperature region of the TPR-S patterns (Fig. 3B), with maximum that shifts from 728 to 947 K with increasing sulfidation temperature, would correspond to RuS_2-pyrite.

It is likely that under reaction conditions ($T = 493$–633 K), in which a rich hydrogen atmosphere prevails, the Ru sulfided species in the low-temperature zone of the TPR-S (overstoichiometric sulfur and RuS_2-amorphous) will be reduced. To analyze this possibility, TPR-S experiments with catalysts tested in HDS reaction for 48 h (Fig. 4) were conducted. Indeed, after reaction, no reduction peaks are observed in the low-temperature zone of the TPR-S patterns, and only the Ru sulfided species that reduce at high temperature (RuS_2-pyrite) are preserved. The TEM results (discussed later) corroborated the presence of pyrite particles at the surface of the catalyst sulfided at 973 K after several hours in HDS reaction (Fig. 9).

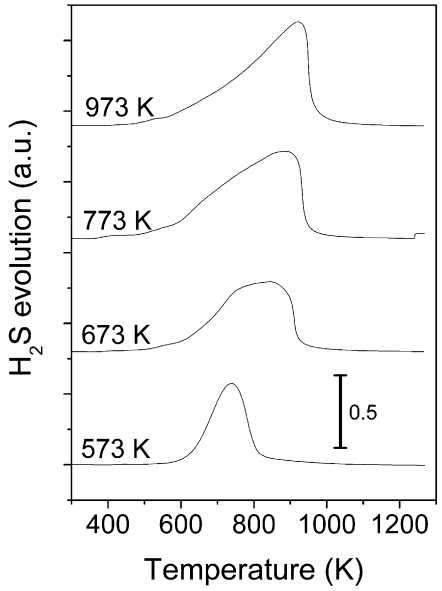

Fig. 4. TPR-S patterns after thiophene HDS of Ru/Al_2O_3 sulfided at 573, 673, 773 and 973 K.

Table 5
S/Ru ratio in catalysts freshly sulfided and after thiophene HDS.

Sulfidation temperature (K)	S/Ru freshly sulfided (TPR-S)	S/Ru after thiophene HDS (TPR-S)	S/Ru after thiophene HDS (SEM-EDS)
573	2.4	1.0	1.0
673	2.4	1.6	1.4
773	2.6	1.8	1.8
973	2.7	2.1	2.0

Quantification of the TPR-S patterns (Figs. 3 and 4) indicated, in agreement with previous reports [16–18], that for freshly sulfided catalysts that contain overstoichiometric sulfur, a S/Ru ratio > 2 is obtained independent of the sulfidation temperature. However, after several hours in thiophene HDS, the S/Ru ratio of the catalysts sulfided below 773 K diminished to values between 1.0 and 1.8 (SEM-EDS), indicating the partial reduction of the Ru phase during the reaction (Table 5). Because overstoichiometric and RuS_2-amorphous are reduced during the HDS reaction and only RuS_2-pyrite prevails on the catalytic surface (see Figs. 3 and 4), the observed variations in catalytic activity with sulfidation temperature (see Tables 1 and 2) suggest that RuS_2-pyrite is strongly active in HDS but has poor naphthalene hydrogenation properties.

The asymmetry of the peak that arises from RuS_2-pyrite reduction for catalysts sulfided at 673–973 K (Fig. 4) is related to surface reduction followed by bulk reduction [23,24]. In the case of sulfidation at 673 K, the reduction consists of two peaks of the same height, but as the sulfidation temperature increases, the proportions between the two peaks change, suggesting decreased sulfur on the surface and increased sulfur on the bulk. The symmetry of the RuS_2-pyrite peak in the catalyst sulfided at 573 K is indicative of reduction in a single step and suggests that the particles associated with this peak do not have pyrite structure in both the

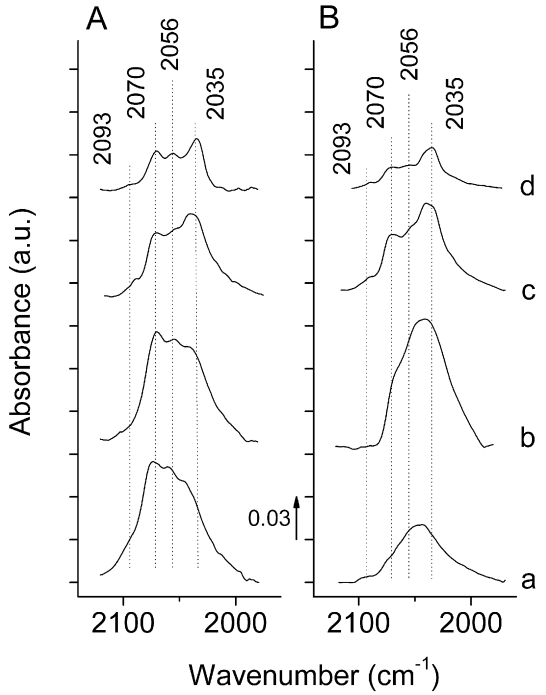

Fig. 5. Spectra of CO adsorbed on Ru/Al_2O_3 sulfided at 573 (a), 673 (b), 773 (c) and 973 K (d). Part A—Freshly sulfided samples. Part B—After treatment emulating HDS reaction conditions.

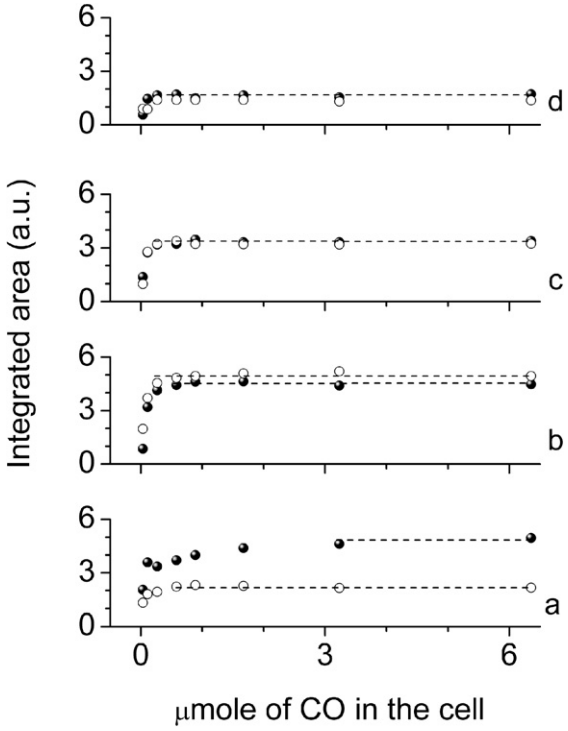

Fig. 6. Integrated area of the CO bands versus amount of CO introduced on the catalysts sulfided at (a) 573 K, (b) 673 K, (c) 773 K, (d) 973 K. (◕) Catalysts freshly sulfided, (○) catalysts after treatment emulating HDS reaction conditions.

bulk and the surface. Because it is more difficult to obtain the pyrite structure in the surface than in the bulk [8,9], it is likely that at this low sulfidation temperature, the surface of the supported particles does not achieve pyrite structure and thus reduces at temperatures much lower than 728 K, along with the reduction of RuS_2-amorphous. This surface reduction in the early stages of the TPR-S gives rise to pyrite particles with sulfur-depleted surfaces that reduce in a single step with maximum at 728 K. Thus, it appears that sulfidation temperatures above 573 K are needed to produce pyrite structure in the surface of supported particles in Ru/Al_2O_3 catalysts.

3.5. Spectroscopic characterization of RuS_2/Al_2O_3

3.5.1. FT-IR spectroscopy of CO adsorbed at low temperature

IR experiments of CO adsorbed at low temperature were conducted to study the evolution of the surface of the RuS_2 particles. CO is a weak base that interacts with the coordinatively unsaturated sites (CUS) of ruthenium and is extremely sensitive to changes in the electronic environment of Ru [32,33].

Fig. 5A presents the infrared spectra of CO adsorbed on the freshly sulfided catalysts. For the catalyst freshly sulfided at 973 K, the spectrum of adsorbed CO presents four bands at 2093, 2070, 2056, and 2035 cm^{-1} (Fig. 5A-d). These bands have been attributed to linear or dicarbonyl CO adsorbed on surface Ru^{2+} with different coordination in sulfur atoms. The band at 2093 cm^{-1} characterizes CO adsorption on Ru cations with high sulfur coordination. The bands at 2056 cm^{-1} and the pair of bands at 2070 and 2035 cm^{-1} characterize the monocarbonyl and dicarbonyl species, respectively, adsorbed on Ru cations with lower sulfur coordination. These two bands are the symmetric and antisymmetric components of a pair of CO molecules adsorbed on the same site [32,33]. The bands in this spectrum are well defined, narrow, and symmetric, suggesting that the surface of the ruthenium sulfide particles is well defined. In contrast, a broad CO spectrum with less well-defined peaks is obtained for the catalyst freshly sulfided at 573 K (Fig. 5A-a). This kind of spectrum may arise from the contribution of several cationic centers with different electronic environments present in the particle surface as a result of a certain degree of disorder in the sulfided phase. The increase in sulfidation temperature from 573 to 973 K results in development of better-defined CO peaks with different relative intensities. This indicates a progressive change in the surface of ruthenium sulfide particles with sulfidation temperature, which can be interpreted as the development of a pyrite-like structure, as shown by the XRD observations (Table 3).

On the surface of a pyrite ruthenium disulfide crystallite, the cations on the face of the cube have the highest sulfur coordination, with only one anion vacancy. Thus, it seems reasonable to assign the vibration at 2093 cm^{-1} to CO adsorbed on the RuS_2 face sites. In the spectra of the freshly sulfided catalysts (Fig. 5A), only a small quantity of CO adsorbs on the cube face sites. The main bands are seen at lower wavenumbers, indicating that CO adsorption occurs mainly on sites with lower sulfur coordination, that is, edge and corner sites. This suggests that the active sites available for HDS reaction are located at the edges and corners of pyrite RuS_2 particles.

Fig. 5B presents the spectra related to CO adsorbed on sulfided samples subjected to reaction-like conditions (treatment at 633 K under flow of $H_2S(15\%)/H_2$). The catalyst sulfided at 973 K shows the same well-defined peaks of the freshly sulfided sample with slightly varying relative intensities (Fig. 5B-d). In contrast, the catalyst sulfided at 573 K has mainly one wide band centered at ∼2040 cm^{-1} (Fig. 5B-a), suggesting strong desulfurization of the surface. This result agrees well with the TPR-S and SEM-EDS experiments showing that thiophene HDS leads to a marked decrease from 2.4 to ∼1 in the S/Ru ratio of the catalyst sulfided at 573 K (Table 5). The spectrum 5B-a does not resemble that of ruthenium sulfide, because it comes from the contribution of strongly desulfurized ruthenium sites with low sulfur coordination. The increase in sulfidation temperature develops the CO peaks associated to RuS_2-pyrite (Fig. 5B).

To quantify the amount of CO adsorbed on the sulfided phase, increasing quantities of CO were contacted with the catalysts freshly sulfided and after reaction-like conditions. Fig. 6 shows the doses of CO introduced on the catalysts versus the integrated area of the bands resulting from CO adsorption on the sulfided phase. The complete titration of all cationic sites in the sulfided phase (represented by the plateau of the integrated area in Fig. 6) occurred before the beginning of CO adsorption on the alumina support, within the first four CO doses (0.58 μmol). The only exception to this behavior occurs in the case of the catalyst freshly sulfided at 573 K, in which the adsorption of CO on the sulfided phase continued at higher CO doses.

The saturation of the cationic sites was reached with 0.58, 0.27, and 0.11 μmol of CO when the catalyst was freshly sulfided at 673, 773, and 973 K, respectively. The greater amount of CO adsorbed on the catalyst sulfided at the lower temperatures indicates that the disordered phase can accommodate more CO than the well-crystallized sulfided phase produced at higher temperatures. This is not surprising, because on the well-crystallized structure, the electronic density from the equally oriented disulfide anions on the cubic structure may inhibit the adsorption of CO. This behavior reinforces the idea that the active sites likely are located on low-coordination sites in corners and edges of the pyrite ruthenium disulfide cubic crystallites, where the adsorption of the sulfur-containing molecule is less inhibited.

Fig. 6 shows that the capability to adsorb CO diminished after reaction-like conditions for the catalysts sulfided at 573, whereas for the catalysts sulfided at higher temperatures the CO uptake on the sulfide phase remained almost the same. The total amount of CO adsorbed on the catalysts after reaction-like conditions followed no trend which could be related to the activity in thiophene HDS or naphthalene hydrogenation. Because the spectra of catalysts sulfided at different temperatures revealed contributions of ruthenium cations in sulfur environment with several coordinations, the lack of correlation between CO adsorbed and catalytic activity indicates that the various Ru sites have different activity toward these two reactions.

The results from these experiments indicate that the surfaces of ruthenium sulfide particles produced by sulfidation from 573 to 973 K differ greatly. The surfaces formed at high sulfidation temperatures (773 and 973 K) are more stable toward the $H_2S(15\%)/H_2$ treatment at 633 K than those formed at lower temperatures (573 and 673 K), which were reduced considerably. According to the literature, once RuS_2-pyrite is formed, it remains unaltered and preserves its sulfided state under hydrogen atmosphere containing only few ppm of H_2S [8,9,11]. This confirms that with sulfidation at 973 K, the surface of the ruthenium sulfide particles acquires pyrite structure, whereas at low sulfidation temperatures, a less well-defined and less stable phase is formed. The increased selectivity toward tetrahydrothiophene observed in the thiophene HDS reaction (Section 3.1) also is in agreement with the progressive formation of pyrite structure with sulfidation temperature [8,9].

3.5.2. Electronic spectroscopy of sulfided catalysts

DRS–UV–Visible–NIR spectroscopy is a powerful technique for studying structure that is widely used to determine the geometry of transition metals in solids. Less common is the use of the electronic spectra to study structural defects. To provide more elements on the co-existence of RuS_2-pyrite and RuS_2-amorphous on RuS_x/Al_2O_3, we performed a detailed DRS–UV–Visible–NIR study on catalysts freshly sulfided at 573, 673, and 973 K.

Ruthenium sulfide is a semiconductor with band gap of 1.3–1.83 eV in RuS_2 single crystals [34–36]. In colloidal particles and RuS_2/SiO_2 suspensions, the band gap of RuS_2 is of 2.3–2.8 [37,38]. The different values of E_g come from differences in particle size; large particles have lower E_g values.

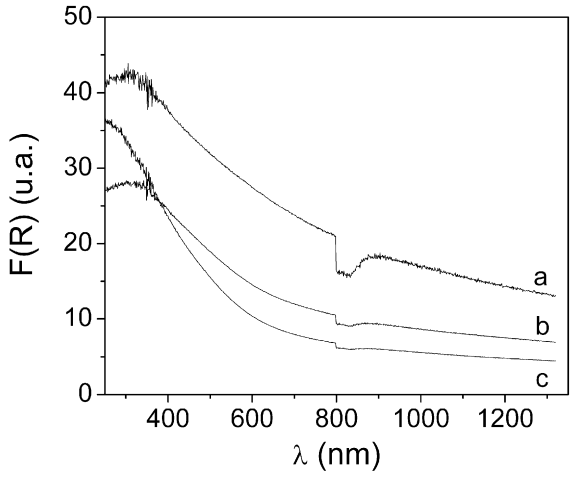

Fig. 7. DRS–UV–Visible–NIR spectra of Ru/Al_2O_3 freshly sulfided in $H_2S(15\%)/N_2$ at 573 K (a), 673 K (b), 973 K (c).

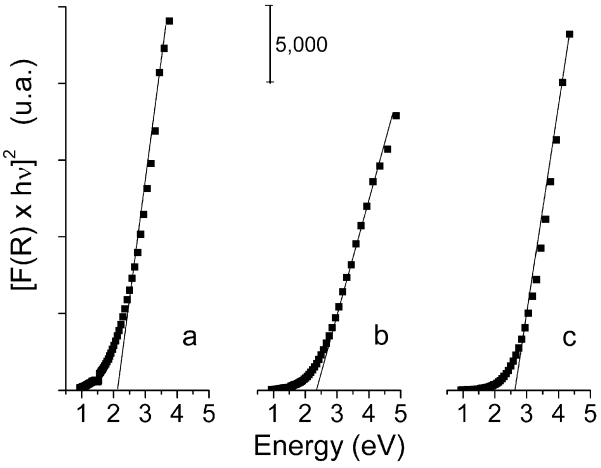

Fig. 8. Absorption edge from DRS–UV–Visible–NIR spectra of Ru/Al_2O_3 freshly sulfided in $H_2S(15\%)/N_2$ at 573 K (a), 673 K (b), 973 K (c).

Fig. 7 reports the absorption electronic spectra of Ru/Al_2O_3 freshly sulfided in $H_2S(15\%)/N_2$ at 573 K (a), 673 K (b), and 973 K (c). In agreement with the behavior observed in other transition metal sulfides [38–40], alumina-supported ruthenium sulfide absorbs energy along the entire reported interval. The absorption at energies below the band gap (2.3–2.8 eV), that is, at wavelengths >443–539 nm, reveals the presence of defects in the sulfided samples, because structural defects give rise to electronic states localized in the band gap and thus to electronic transitions at energies below the band gap from the valence band toward electronic states associated with defects [41]. The trend in absorption at energies below the band gap ($\lambda > 443$–539 nm), for example, $F(R) = 4.5, 7$, and 13.2 at 1300 nm for Ru/Al_2O_3 sulfided at 973, 673, and 573 K, respectively, indicates that the catalyst sulfided at low temperature (573 K) has more defects and that the increased sulfidation temperature diminishes the number of defects in the catalyst surface.

Fig. 8 shows the absorption edge for the catalysts sulfided at 573, 673, and 973 K. All samples had a defined absorption edge with values of 2.1, 2.3, and 2.6 eV, respectively, in accordance with literature reports for RuS_2-supported particles [38]. In the sample sulfided at 573 K (Fig. 8a), along with the absorption edge, an increasing absorption from 0.9 to 2.1 eV is observed. The continuous absorption below 2.1 eV arises from electronic transitions to localized states and indicates that the sulfided catalyst is highly de-

Table 6
H_2S evolved from the reduction of 150 mg of sulfided catalyst (0.104 mmoles of ruthenium) after thiophene HDS.

Sulfidation temperature (K)	Total H_2S evolved (mmol)	mmole of Ru in RuS_2	Percent of Ru as RuS_2-pyrite
573	0.10	0.05	47
673	0.16	0.08	75
773	0.18	0.09	86
973	0.21	0.10	100

fective, because the shape of the absorption edge corresponds well with that of an amorphous solid [41]. In contrast, for the sample sulfided at 973 K (Fig. 8c), an energy zone between 0.95 and ∼2 eV with no increment in absorption, followed by the beginning of an absorption edge, indicates that the spectrum comes from a crystalline solid. Therefore, the DRS–UV–Visible–NIR experiments show that a highly defective ruthenium sulfide is obtained at low sulfidation temperature, whereas a more crystalline ruthenium sulfide phase with fewer defects is produced when the sulfidation temperature is increased.

In summary, all of the characterizations of Ru/Al_2O_3 sulfided in $H_2S(15\%)/N_2$ at $573 < T < 973$ K presented above show that high temperature is needed to induce the crystallization of RuS_2-pyrite. A catalyst with greater number of defects—RuS_2-amorphous—is produced at low sulfidation temperature. With sulfidation at 973 K, even the surface of the ruthenium sulfide particles acquires pyrite structure, whereas at low sulfidation temperature, a less defined and less stable phase is formed.

3.6. Quantification of RuS_2-amorphous and RuS_2-pyrite in the Ru/Al_2O_3 catalyst

Quantification of the amounts of RuS_2-amorphous and RuS_2-pyrite in the Ru/Al_2O_3 catalyst was made by three different methods: (i) deconvoluting the TPR-S patterns of freshly sulfided catalysts, (ii) relating the measured amount of H_2S evolved from the reduction of the catalyst exposed to reaction conditions with the ruthenium load, and (iii) evaluating the S/Ru ratio by SEM-EDS in catalysts exposed to reaction. Deconvolution of the TPR-S patterns of freshly sulfided catalysts (Fig. 3), where peaks of both RuS_2-amorphous (peak at ∼513 K) and RuS_2-pyrite (peak at 728–947 K) are present, reveals that 47, 63, 87, and 94% of the sulfided species is in the form of RuS_2-pyrite and 53, 37, 13, and 6% is in the form of RuS_2-amorphous when the Ru/Al_2O_3 catalyst is sulfided at 573, 673, 773, and 973 K, respectively.

As the characterizations show, after HDS reaction, only RuS_2-pyrite remains as a sulfided phase in the catalysts. Therefore, the amount of RuS_2-pyrite was determined from the amount of H_2S (mmole) evolved from the reduction of the catalysts after reaction (Fig. 4) and the ruthenium load (0.104 mmoles in 150 mg of catalyst). Table 6 shows that the H_2S produced during the reduction of the catalyst sulfided at 973 K corresponds to the ruthenium load in S/Ru = 2 stoichiometry, indicating that for this catalyst, 100% of the ruthenium load is in the form of RuS_2-pyrite. In contrast, only 47, 75, and 86% of the 0.104 mmoles of ruthenium is in the form of RuS_2-pyrite when the catalyst is sulfided at 573, 673, and 773 K, respectively. These results are in good agreement with those obtained from deconvolution of the TPR-S traces of freshly sulfided catalysts.

Finally, the S/Ru ratio determined by SEM-EDS in catalysts exposed to reaction also provides a measure of the amount of RuS_2-pyrite. The catalyst sulfided at 973 K has an S/Ru ratio of 2.0, indicating that practically all of the ruthenium in the catalyst forms part of RuS_2-pyrite. The S/Ru ratios of 1.0, 1.4, and 1.8 reported in Table 5 for catalysts sulfided at 573, 673, and 773 K, respectively, correspond to 49.5, 68.5, and 88% of the stoichiometric ratio

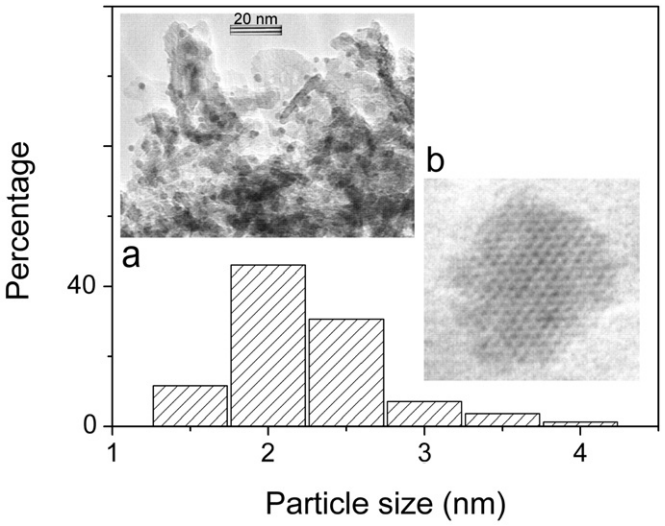

Fig. 9. Particle size distribution in Ru/Al_2O_3 sulfided at 973 K after 15 h in HDS reaction at 633 K. Average size = 2.2 nm. (a) TEM micrograph. (b) Hexagonal atomic distribution in the (111) face of a 4.3 nm ruthenium sulfide particle.

S/Ru = 2 as well as to the percent of pyrite present after reaction conditions.

The similarity of the three methods of estimating the relative amounts of RuS_2-pyrite and RuS_2-amorphous (obtained by difference from the total load of Ru) reinforces the validity of the results.

The (mole of RuS_2-pyrite)/(mole of RuS_2) ratio measured at each sulfidation temperature by SEM-EDS was used to transform the HDS rates from molecules of thiophene $*$ second^{-1} $*$ (ruthenium atom)$^{-1}$ (Table 1) to molecules of thiophene $*$ second^{-1} $*$ (ruthenium atom in RuS_2-pyrite)$^{-1}$. The rates obtained are 0.3, 1.4, 1.5, and 1.7×10^{-3} molecules of thiophene s^{-1} (Ru atom in RuS_2-pyrite)$^{-1}$ at the sulfidation temperatures of 573, 673, 773 and 973 K, respectively. This result reinforces the assignation of RuS_2-pyrite as the active phase in HDS since the last three rates are similar. The low activity of the catalyst sulfided at 573 K may be a consequence of the lack of pyrite structure at the surface of the ruthenium sulfide particles, as evidenced by TPR-S (Section 3.4).

The constancy of the HDS rates obtained at higher sulfidation temperatures (673, 773 and 973 K) indicates no significant change in the ruthenium sulfide particle size with sulfidation temperature. To rationalize this result a TEM study was conducted with the catalysts sulfided at 573, 773 and 973 K after 15 h of thiophene HDS reaction at 633 K. As an example, Fig. 9 shows the particle size distribution for the catalyst sulfided at 973 K. The TEM study showed that only a slight increment in particle size is obtained with the increase of the sulfidation temperature: the average particle size changes from 2.0 to 2.2 nm when the temperature varies from 573 to 973 K. Based on the model in [24] the percentage of ruthenium atoms in edges and corners in ruthenium sulfide particles of 2.0 and 2.2 nm is $\sim 13.5 \pm 5\%$. The small increment in particle size along with the small variation in the number of active sites can explain why the catalytic activity expressed as molecules of thiophene $*$ second^{-1} $*$ (ruthenium atom in RuS_2-pyrite)$^{-1}$ does not significantly change with the increase in the sulfidation temperature.

With the use of a small molecule such as thiophene, that can reach without impediments the active sites in ruthenium sulfide, it was possible to relate the structural changes induced by the increase of the sulfidation temperature and the extent of desulfurization during the reaction with the HDS activity of the ruthenium sulfide phase. Activity tests performed with batch reactor in the HDS of dibenzothiophene (DBT) showed that the HDS initial activity increases from 4×10^{-12} to 7×10^{-12} molecule DBT $s^{-1}\,m^{-2}$

when the sulfidation temperature increases from 673 to 973 K. It can be seen that the activity in DBT HDS is lower than that of thiophene HDS but that the activity trend with sulfidation temperature is similar. This suggests the same behavior of the ruthenium sulfide with the two sulfur containing molecules.

3.7. Hydrodesulfurization versus hydrogenation

The results presented up to here showed that RuS_2-pyrite and RuS_2-amorphous are formed during sulfidation with $H_2S(15\%)/N_2$. The increase in sulfidation temperature induced RuS_2-pyrite crystallization, in detriment of RuS_2-amorphous. During the HDS reaction RuS_2-amorphous is reduced while RuS_2-pyrite remains stable on the catalytic surface.

The reduction of amorphous ruthenium sulfide during the thiophene HDS reaction causes the decrease of the S/Ru > 2 ratio displayed by the freshly sulfided catalysts (Table 5). Understandably, the S/Ru ratio in the catalyst after thiophene HDS (measured by TPR-S and SEM-EDS, Table 5) increases with sulfidation temperature from S/Ru ∼ 1 ($T = 573$ K) to S/Ru ∼ 2 ($T = 973$ K). This result is important since it shows that the reduction of the amorphous ruthenium sulfide during reaction leads to a sulfur depleted catalyst, with low S/Ru ratio and poor HDS activity (Tables 5 and 1). The catalyst sulfided at 973 K, which retains the stoichiometric S/Ru ratio of 2 in reaction, is ten times more active in HDS than the one sulfided at 573 K. Therefore, our results show that the HDS activity of supported ruthenium sulfide increases with the extent of sulfidation (higher S/Ru ratio) at reaction conditions.

The hydrogenation of thiophene to produce tetrahydrothiophene follows the same trend as hydrodesulfurization and the RuS_2-pyrite phase obtained at 973 K, with S/Ru ∼ 2 in reaction, is the most active catalyst (Section 3.1). On the contrary, the kinetic coefficient in the hydrogenation of naphthalene reported in Table 2 follows an opposite trend. To explain this apparent contradiction, the different surface structures and composition in each case must be considered. In the catalyst sulfided at high temperature with pyrite structure on the surface (S/Ru = 2 in reaction), there are S pairs able to dissociate hydrogen [8], that can be transferred to the thiophene molecules bonded to ruthenium CUS through the sulfur atom [42], making the catalyst very active in the hydrogenation of thiophene. In the case of naphthalene, adsorption in the catalytic surface proceeds through the π cloud [42]. In this case, it is likely that the S pairs in the pyrite surface inhibit the adsorption of the aromatic ring, resulting in low catalytic activity. In contrast, the unstable ruthenium sulfide catalyst that results from sulfidation at low temperature does not present impediment to naphthalene adsorption since during reaction sulfur is removed from the surface of the ruthenium sulfide particles by hydrogen. The formation of some Ru^0 due to the partial reduction of the catalyst will also favor the hydrogenation of naphthalene molecules [29]. The hydrogenation of thiophene is not favored in this highly desulfurized surface probably due to sulfur poisoning of the metallic Ru atoms exposed to reaction.

This result shows that to hydrogenate sulfur containing molecules with the intention of favoring its hydrodesulfurization, the ruthenium sulfide catalyst must have pyrite structure, that is, has to be sulfided at high temperature and preserve a S/Ru ratio close to 2 in reaction. In contrast, to hydrogenate aromatic molecules such as naphthalene, a partially reduced catalyst (sulfided at low temperature in $H_2S(15\%)/N_2$) will perform better.

3.8. Effect of hydrogen during sulfidation

It is well documented that sulfidation in the presence of hydrogen originates a sulfided RuS_x phase with S/Ru < 2 and low HDS activity [15]. On the other hand, this work has shown that sulfidation in the absence of hydrogen at low temperature produces a well sulfided (S/Ru > 2) but unstable phase that undergoes partial reduction at HDS reaction conditions. Additional TPR-S experiments were performed with Ru/Al_2O_3 sulfided with $H_2S(15\%)/H_2$ to study the characteristics of the active phase compared to those of RuS_2 sulfided in the absence of hydrogen at low temperature.

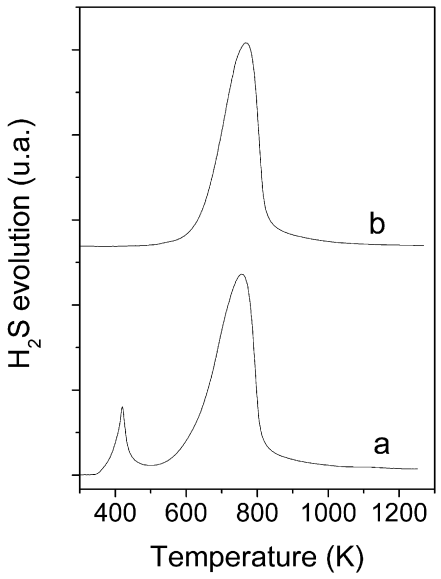

Fig. 10. TPR-S of Ru/Al_2O_3 (a) freshly sulfided in $H_2S(15\%)/H_2$ at 673 K, (b) after thiophene HDS.

Fig. 10 reports the reduction patterns of a catalyst freshly sulfided at 673 K in $H_2S(15\%)/H_2$ (Fig. 10a), and after 48 h of thiophene hydrodesulfurization (Fig. 10b). The S/Ru ratio in the freshly sulfided catalyst equals 1.5 (against 2.35 in the catalyst sulfided with $H_2S(15\%)/N_2$). The S/Ru ratio in the catalyst subjected to reaction conditions is 1.3. These results are in line with TPR-S measurements that reported different levels of sulfidation in catalysts sulfided with or without hydrogen in the sulfidation stream [43] and a strong decrement in the S/Ru ratio in reaction with catalysts sulfided in the presence of hydrogen [44].

After thiophene HDS, the characteristics of Ru/Al_2O_3 sulfided in $H_2S(15\%)/H_2$ at 673 K are similar to those in the catalyst sulfided in $H_2S(15\%)/N_2$ at 573 K. The shape of the reduction pattern (Figs. 10b and 4), the S/Ru ratio (1.3 vs 1), the reaction rate (0.13×10^{-3} vs 0.17×10^{-3} molecule of thiophene/sec-Ru atom), and the selectivity (1.6 vs 1.7) were practically the same.

According to these results, sulfidation in the absence of hydrogen at low temperature (573 K) leads to a well sulfided but highly defective Ru sulfided phase, which is unstable and reduces under reaction conditions, resulting in a low S/Ru ratio phase with poor catalytic performance in hydrodesulfurization. This phase is similar to that obtained by sulfiding with $H_2S(15\%)/H_2$ at 673 K. This result is important, because it shows that the desulfurized ruthenium sulfide phase displays low HDS activity, formed either during sulfidation with hydrogen or by reduction during the HDS reaction.

4. Conclusion

Sulfidation of Ru/Al_2O_3 in $H_2S(15\%)/N_2$ at temperatures between 573 and 973 K was found to lead to a fully sulfided phase consisting of a mixture of RuS_2-amorphous and RuS_2-pyrite. The increment in sulfidation temperature favors the formation RuS_2-pyrite to the detriment of RuS_2-amorphous. These ruthenium sulfide phases behave differently in HDS reaction conditions. RuS_2-pyrite is stable and displays high HDS activity, whereas RuS_2-

amorphous undergoes reduction producing a sulfur depleted active phase with a S/Ru ratio much lower than 2, that displays poor HDS activity, similar to that obtained by sulfidation with $H_2S(15\%)/H_2$. So, the HDS activity increases with the extent of sulfidation of the ruthenium sulfide phase present at reaction conditions.

In naphthalene hydrogenation, the activity trend is opposite to HDS: the catalyst sulfided at low temperature with low S/Ru ratio in reaction displays the best catalytic performance. But the desulfurized phase does not perform well in the hydrogenation of a sulfur-containing molecule such as thiophene. In contrast, hydrogenation of thiophene is more easily achieved with a fully sulfided RuS_2-pyrite phase.

Our findings demonstrate that the structure of the ruthenium sulfide catalyst can be tuned during the sulfidation to achieve optimum performance according to the hydrodesulfurization or hydrogenation requirements of the reaction system.

Acknowledgments

We are indebted to DGAPA–UNAM program for financial support. We acknowledge Cecilia Salcedo for the XRD experiments, Ivan Puente for the SEM-EDS and TEM observations, Leticia Baños for helpful discussions and Rogelio Cuevas for his help in the reaction experiments.

References

[1] T.A. Pecoraro, R.R. Chianelli, J. Catal. 67 (1981) 430.
[2] A.P. Raje, S.-J. Liaw, R. Srinivasan, B.H. Davis, Appl. Catal. A 150 (1997) 297.
[3] M. Lacroix, H. Marrakchi, C. Calais, M. Breysse, C. Forquy, Stud. Surf. Sci. Catal. 59 (1991) 227.
[4] N. Hermann, M. Brorson, H. Topsøe, Catal. Lett. 65 (2000) 169.
[5] M. Lacroix, N. Boutarfa, C. Guillard, M. Vrinat, M. Breysse, J. Catal. 120 (1989) 473.
[6] R.A. Cocco, B.J. Tatarchuk, Langmuir 5 (1989) 1309.
[7] W.H. Heise, K. Lu, Y.-J. Kuo, T.J. Udovic, J.J. Rush, B.J. Tatarchuk, J. Phys. Chem. 92 (1988) 5184.
[8] Y.-J. Kuo, R.A. Cocco, B.J. Tatarchuk, J. Catal. 112 (1988) 250.
[9] Y.-J. Kuo, B.J. Tatarchuk, J. Catal. 112 (1988) 229.
[10] K. Lu, Y.-J. Kuo, B.J. Tatarchuk, J. Catal. 116 (1989) 373.
[11] M. Zdrazil, Catal. Today 3 (1988) 269.
[12] J.A. De Los Reyes, Appl. Catal. A 322 (2007) 106.
[13] J.A. De Los Reyes, S. Göbölös, M. Vrinat, M. Breysse, Catal. Lett. 5 (1990) 17.
[14] S. Göbölös, M. Lacroix, T. Decamp, M. Vrinat, M. Breysse, Bull. Soc. Chim. Belg. 100 (1991) 907.
[15] B. Moraweck, G. Bergeret, M. Cattenot, V. Kougionas, C. Geantet, J.L. Portefaix, J.L. Zotin, M. Breysse, J. Catal. 165 (1997) 45.
[16] J.A. De Los Reyes, M. Vrinat, C. Geantet, M. Breysse, Catal. Today 10 (1991) 645.
[17] C. Dumonteil, M. Lacroix, C. Geantet, H. Jobic, M. Breysse, J. Catal. 187 (1999) 464.
[18] J.A. De Los Reyes, M. Vrinat, C. Geantet, M. Breysse, J.G. Grimblot, J. Catal. 142 (1993) 455.
[19] O. Knop, Can. J. Chem. 41 (1963) 1832.
[20] O. Sutarno, O. Knop, K.I.G. Reid, Can. J. Chem. 45 (1967) 1391.
[21] H.D. Lutz, B. Müller, T. Schmidt, T. Stingl, Acta Crystallogr. Sect. C: Cryst. Struct. Commun. C 46 (1990) 2003.
[22] G. Berhault, M. Lacroix, M. Breysse, F. Maugé, J.C. Lavalley, L. Qu, J. Catal. 170 (1997) 37.
[23] F. Lebruyère, M. Lacroix, D. Schweich, M. Breysse, J. Catal. 167 (1997) 464.
[24] C. Geantet, C. Calais, M. Lacroix, C. R. Acad. Sci. Paris 315 (1992) 439.
[25] V. Kougionas, M. Cattenot, J.L. Zotin, J.L. Portefaix, M. Breysse, Appl. Catal. A 124 (1995) 153.
[26] M. Lacroix, C. Dumonteil, M. Breysse, Prepr. Am. Chem. Soc., Div. Pet. Chem. (1998) 35.
[27] M. Wojciechowska, M. Pietrowski, B. Czajka, S. Lomnicki, Catal. Lett. 87 (2003) 153.
[28] J.L. Zotin, M. Cattenot, J.L. Portefaix, M. Breysse, Actas XIV Simp. Iberoamericano de Catálisis (1994) 1431.
[29] J. Blanchard, K.K. Bando, T. Matsui, M. Harada, M. Breysse, Y. Yoshimura, Appl. Catal. A 322 (2007) 98.
[30] J.D. Passaretti, R.B. Kaner, R. Kershaw, A. Wold, Inorg. Chem. 20 (1980) 501.
[31] A. Ishiguro, T. Nakajima, T. Iwata, M. Fujita, T. Minato, F. Kiyotaki, Y. Izumi, K.-I. Aika, M. Uchida, K. Kimoto, Y. Matsui, Y. Wakatsuki, Chem. Eur. J. 8 (2002) 3260.
[32] K. Hadjiivanov, J.C. Lavalley, J. Lamotte, F. Maugé, J. Saint-Just, M. Che, J. Catal. 176 (1998) 415.
[33] G. Berhault, F. Maugé, J.C. Lavalley, M. Lacroix, M. Breysse, J. Catal. 189 (2000) 431.
[34] H. Ezzaouia, R. Heindl, R. Parsons, H. Tributsch, J. Electroanal. Chem. 145 (1983) 279.
[35] H.-M. Kühne, H. Tributsch, J. Electroanal. Chem. 201 (1986) 263.
[36] R. Bichsel, F. Levy, H. Berger, J. Phys. C 17 (1984) L19.
[37] M. Ashokkumar, A. Kudo, T. Sakata, Bull. Chem. Soc. Jpn. (1995) 2491.
[38] K. Hara, K. Sayama, H. Arakawa, Appl. Catal. A 189 (1999) 127.
[39] J. Ramírez, L. Cedeño, G. Busca, J. Catal. 184 (1999) 59.
[40] C.B. Roxlo, M. Daage, A.F. Ruppert, R.R. Chianelli, J. Catal. 100 (1986) 176.
[41] W. Hayes, A.M. Stoneham, Defects and Defects Processes in Nonmetallic Solids, Dover Publications, Mineola, NY, 2004, p. 386.
[42] B.S. Clausen, H. Topsøe, F.E. Massoth, Hydrotreating Catalysis, Springer, Berlin, 1996, p. 131.
[43] M. Wojciechowska, M. Pietrowski, B. Czajka, Catal. Today 65 (2001) 349.
[44] A. Ishihara, M. Nomura, T. Kabe, J. Catal. 150 (1994) 212.